

## CHAPTER 3

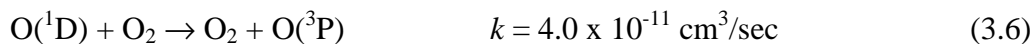
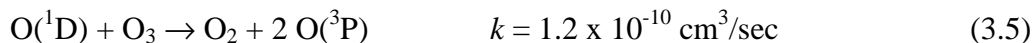
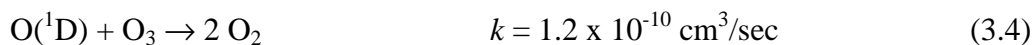
### DATA AND RESULTS

#### **3.1 Kinetic Analysis**

The chemical chain process is initiated by pulsed laser photolysis of O<sub>3</sub> at 308 nm, thus creating O(<sup>1</sup>D) atoms. These excited O(<sup>1</sup>D) atoms rapidly react with water<sup>1-3</sup> and hydrogen<sup>4-7</sup> in the flow cell to yield both vibrationally “hot” (i.e., v>0) and “cold”(i.e., v=0) OH radicals. These studies<sup>1-3</sup> have shown that the ratio of OH(v=1) to OH(v=0) resulting from reaction 3.1 is approximately 0.40. In addition, studies<sup>4-7</sup> of the OH vibrational distribution resulting from reaction 3.3 have shown a distribution in which 80% of the OH population is in v ≥ 7.



There is also rapid competition to quench or react the O(<sup>1</sup>D) species with O<sub>3</sub> ( $k = 2.4 \times 10^{-10} \text{ cm}^3 \text{ molecule}^{-1} \text{ s}^{-1}$ ) or O<sub>2</sub> ( $k = 3.2 \times 10^{-11} \text{ cm}^3 \text{ molecules}^{-1} \text{ s}^{-1}$ ) to yield ground state oxygen atoms or molecules via<sup>8-10</sup>



Since the high-resolution IR laser samples on  $\text{P}(5/2)1^-$  transitions out of OH ( $v=0, J=2.5$ ), the early time signals reflect only the fraction of vibrationally “cold” OH radicals. Rovibrational cooling of the “hot” OH species by collisions with  $\text{H}_2\text{O}$  and Ar buffer gas rapidly brings the system to room temperature equilibration. Under typical flow cell conditions, rapid quenching of these rovibrationally “hot” OH radicals, results in an essentially “prompt” rise in OH signals probed out of the  $v = 0$ , low  $N$  quantum levels, which on a much longer timescale, reacts with  $\text{O}_3$  to initiate the chemical chain reaction cycle (see figure 3-1). The key point is that the OH populations are equilibrated to a temperature distribution on  $<5 \mu\text{s}$  time scale, which is 1 or 2 orders of magnitude faster than the subsequent chain reaction kinetics under investigation.

Thus, for the purposes of kinetic analysis, initiation of the chain reaction can be approximated simply by prompt generation of  $[\text{OH}]_0$  at  $t = 0$ . For typical XeCl pulse energies and beam sizes,  $[\text{OH}]_0$  is 3 or 4 orders of magnitude smaller than  $[\text{O}_3]$ , which is necessary to ensure a pseudo-first-order kinetic regime and discriminate against radical-radical termination reactions. In this limit, the relevant coupled kinetic equations become

$$\frac{d[\text{OH}]}{dt} = -k_1[\text{OH}][\text{O}_3] + k_2[\text{HO}_2][\text{O}_3] \quad (3.7)$$

$$\frac{d[\text{HO}_2]}{dt} = k_1[\text{OH}][\text{O}_3] - k_2[\text{HO}_2][\text{O}_3] \quad (3.8)$$

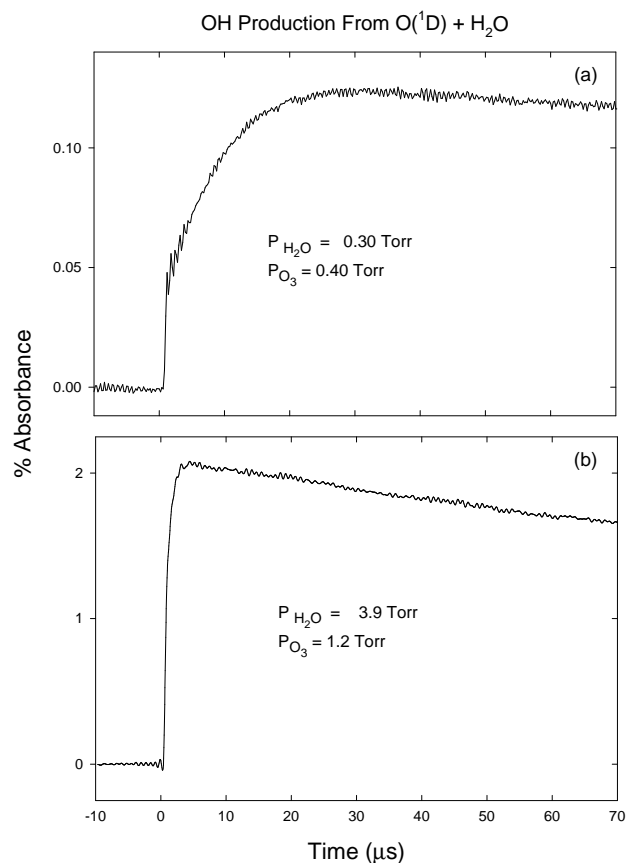


Figure 3-1. OH time profiles measured via time-resolved IR laser absorption on the  $v=1 \leftarrow 0$ ,  $P(2.5)1^-$  transition. In a and b, the buffer gas conditions are chosen to modify the rate of collisional relaxation of the OH radicals, which in effect samples the early time scale dynamics for OH production. (a) At the lowest H<sub>2</sub>O quenching gas concentrations, there is a “prompt” component of OH( $v=0$ ) absorption due to rapid reaction of O(<sup>1</sup>D) with H<sub>2</sub>O, which then rises to roughly twice this value with subsequent collisions in the buffer gas. This nearly 2-fold additional increase in OH signal reflects that vibrationally “hot” (i.e.,  $v > 0$ ) and “cold” OH( $v=0$ ) radicals are generated in roughly equal numbers, corresponding to “active” and “spectator” OH bonds in the O(<sup>1</sup>D) + H<sub>2</sub>O reaction. (b) For typical H<sub>2</sub>O concentrations, however, this collisional relaxation is too rapid to distinguish these two components. The net effect is a prompt production of collisionally equilibrated OH radicals on the 5 μs time scale, which is much faster than the subsequent OH/HO<sub>2</sub>/O<sub>3</sub> chain reaction kinetics of interest.

$$\frac{d[\text{OH}]}{dt} + \frac{d[\text{HO}_2]}{dt} = 0, \quad (3.9)$$

where the last expression reflects the neglect of any net loss of chain radical concentration due to slow wall losses, diffusion out of beam, etc. These kinetic equations can be readily solved for  $[\text{OH}](t)$  and  $[\text{HO}_2](t)$  to yield

$$\frac{[\text{OH}](t)}{[\text{OH}]_0} = \frac{k_1}{k_1 + k_2} e^{-k_{\text{ind}} [\text{O}_3] t} + \frac{k_2}{k_1 + k_2} \quad (3.10)$$

$$\frac{[\text{HO}_2](t)}{[\text{OH}]_0} = \frac{k_1}{k_1 + k_2} \left( 1 - e^{-k_{\text{ind}} [\text{O}_3] t} \right), \quad (3.11)$$

where the effective chain induction rate and steady-state concentrations of OH radical and steady-state rate of chain propagation are given by

$$k_{\text{ind}} = k_1 + k_2 \quad (3.12)$$

$$[\text{OH}]_{\text{ss}} = [\text{OH}]_0 \frac{k_2}{k_1 + k_2} \quad (3.13)$$

$$k_{\text{prop}} = \frac{k_1 k_2}{k_1 + k_2} [\text{O}_3]. \quad (3.14)$$

Equation (3.10) for the time dependence of  $[\text{OH}]$  illustrates several important points. First of all,  $[\text{OH}](t)$  starts initially at  $[\text{OH}]_0$  and undergoes single-exponential decay to a nonzero baseline value of  $[\text{OH}]_{\text{ss}} = [\text{OH}]_0 \frac{k_2}{k_1 + k_2}$ , with a chain “induction” time constant  $\tau_{\text{ind}} = \{k_{\text{ind}} [\text{O}_3]\}^{-1}$ . This induction time constant reflects the time required for OH and HO<sub>2</sub> radicals to come into steady state, and therefore is controlled by the magnitude of *both* chain propagation steps. Consequently, any kinetic analysis of this exponential time dependence yields the *sum* of the two pseudo-first-order propagation rate constants,  $k_1$  and  $k_2$ . This is different from previous kinetic analyses<sup>11-13</sup> of OH + O<sub>3</sub> reaction rates, which

neglect the slower second chain step and ascribe the observed time dependence entirely to  $1/\tau_{\text{ind}} \approx k_1[\text{O}_3]$ . Secondly, the OH decays to a *nonzero value* at  $t \gg \tau_{\text{ind}}$  due to chain regeneration of OH from the secondary  $\text{HO}_2 + \text{O}_3$  reaction. This also differs from previous analyses of  $\text{OH} + \text{O}_3$  kinetics, which treat the OH signal as a *single* exponential decay down to  $[\text{OH}]_{\text{ss}} \approx 0$  and ascribe this time constant to the first step in the chain reaction sequence. Sample chain reaction data supporting this more complete kinetic analysis are presented in figure 3-2, where the water and ozone reagent concentrations are listed in the figure caption.

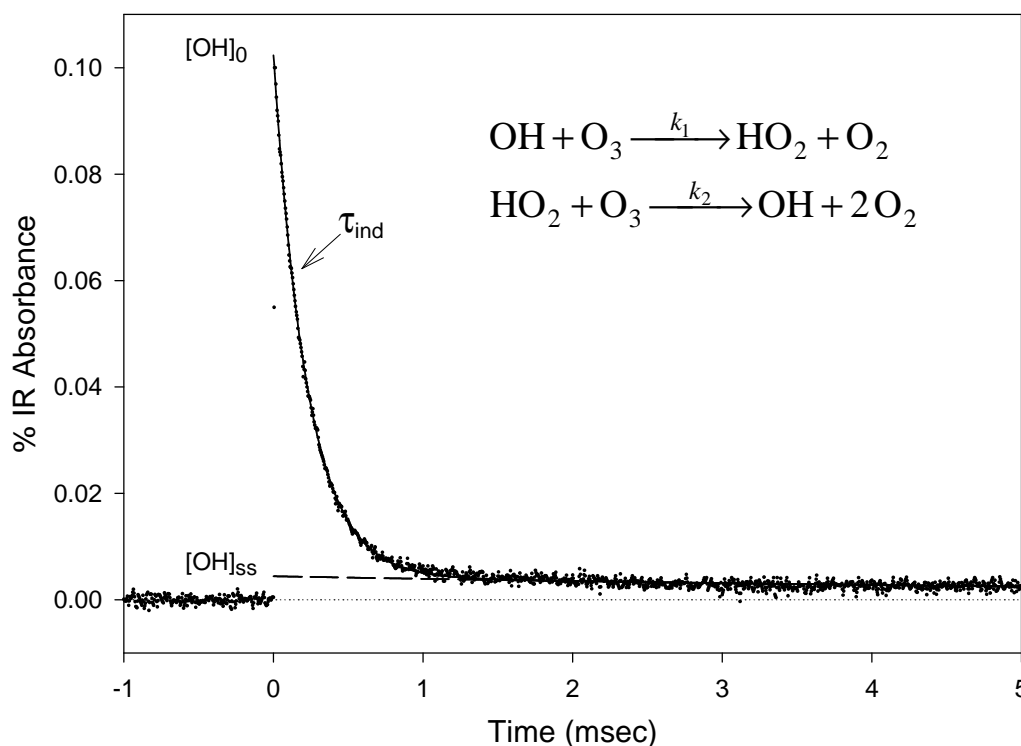


Figure 3-2. Typical OH absorbance data. The fast initial decay signals the “induction” of the chain reaction, followed by a much slower decay from the steady state “propagation” regime to chain termination processes. The fast decay is determined by the sum of the two chain rate constants, whereas the ratio of fast- to slow-decay components reflects the ration of the two chain rate constants. For this data,  $[\text{O}_3] = 1.95$  Torr,  $[\text{H}_2\text{O}] = 5.22$  Torr,  $[\text{Ar}] = 19$  Torr, and the excimer pulse energy is  $0.5 \text{ mJ/cm}^2$  per pulse.

As predicted, the data unambiguously demonstrates single exponential decay from  $[\text{OH}]_0$  to a *finite*  $[\text{OH}]_{\text{ss}}$  plateau, which in turn decays on a much longer time scale ( $t_{\text{decay}} \geq 10$  ms) due to a combination of nonlinear chain termination and diffusion out of the probe laser IR beam volume. Though this secondary decay is due to chain termination and therefore not predicted by the simple chain model, it can be easily treated by including *irreversible* (i.e., non-chain reaction sustaining) loss processes for OH and HO<sub>2</sub>, as presented below.

If we assume first-order, irreversible loss mechanisms for OH and HO<sub>2</sub> radicals, the relevant kinetic equations are modified to become

$$\frac{d[\text{OH}]}{dt} = -k_1[\text{OH}][\text{O}_3] + k_2[\text{HO}_2][\text{O}_3] - k_{\text{irr}}^{\text{OH}}[\text{OH}], \quad (3.15)$$

$$\frac{d[\text{HO}_2]}{dt} = k_1[\text{OH}][\text{O}_3] - k_2[\text{HO}_2][\text{O}_3] - k_{\text{irr}}^{\text{HO}_2}[\text{HO}_2], \quad (3.16)$$

$$\frac{d[\text{OH}]}{dt} + \frac{d[\text{HO}_2]}{dt} = -k_{\text{irr}}^{\text{OH}}[\text{OH}] - k_{\text{irr}}^{\text{HO}_2}[\text{HO}_2]. \quad (3.17)$$

Efficient propagation occurs when irreversible loss of OH and HO<sub>2</sub> is *slow*, and thus the chain reaction is sustained for many cycles. This is kinetically equivalent to saying that the OH/HO<sub>2</sub> ratio is maintained in a steady-state ratio  $k_2/k_1$ , even as both chain radical species are eventually consumed irreversibly. In this simplifying limit of  $k_{\text{irr}}^{\text{OH}}, k_{\text{irr}}^{\text{HO}_2} \ll k_{\text{ind}}$ , equations (3.15-3.17) can be solved to yield

$$\frac{[\text{OH}](t)}{[\text{OH}]_0} = \frac{k_1}{k_1 + k_2} e^{-k_{\text{ind}}[\text{O}_3]t} + \frac{k_2}{k_1 + k_2} e^{-k_{\text{term}}t}. \quad (3.18)$$

This now correctly predicts a *double*-exponential decay in the OH signal, with the faster chain induction component given by  $k_{\text{ind}}$  and a slower chain *termination* component given by

$$k_{\text{term}} = \frac{k_{\text{irr}}^{\text{OH}} k_2}{k_1 + k_2} + \frac{k_{\text{irr}}^{\text{HO}_2} k_1}{k_1 + k_2}. \quad (3.19)$$

It is interesting to note from equation 3.18 that the chain termination rate reflects a *sum of both* OH and HO<sub>2</sub> loss rates, but now weighted by the fractional steady-state concentrations of each radical. As a result, these OH/HO<sub>2</sub>/O<sub>3</sub> chains can still propagate quite efficiently even in the presence of relatively fast irreversible removal processes for OH, due simply to the fact that the *overall* concentration of chain radicals (i.e., [OH] + [HO<sub>2</sub>]) is “stored” as the less reactive HO<sub>2</sub> radical. Note also that this model predicts the *ratio* of  $k_1/k_2$  to be determined by the relative amplitudes of the fast- and slow-decay components back extrapolated to  $t = 0$ . Finally, the total number of chain cycles is typically dominated by the long time propagation behavior, which can be found by integration of equation (3.18) to yield

$$N_{\text{cycles}} \approx \frac{k_{\text{prop}}}{k_{\text{term}}} = \frac{k_1 k_2 [\text{O}_3]}{k_{\text{irr}}^{\text{OH}} k_2 + k_{\text{irr}}^{\text{HO}_2} k_1}. \quad (3.20)$$

In summary, the above kinetic analysis makes three predictions. (1) In the limit of efficient chain propagation and slow chain termination processes, double-exponential time dependence of the OH chain radicals is anticipated. (2) A plot of the fast decay rate vs [O<sub>3</sub>] will yield a slope of  $\{k_1 + k_2\}$  (i.e., the *sum* of the two chain propagation reaction rate constants). (3) The ratio of back extrapolated components for fast (induction) and slow (termination) decays yields  $k_1/k_2$  (i.e., the ratio of the two chain propagation rate constants). A table of relevant reactions occurring in the flow cell are presented in table 3-1.

Reaction	$k[298\text{K}]$ ( $\text{cm}^3/\text{sec}$ )	Reference
$\text{O}(^1\text{D}) + \text{H}_2 \rightarrow \text{OH} + \text{H}$	$1.0 \times 10^{-10}$	14
$\text{O}(^1\text{D}) + \text{H}_2\text{O} \rightarrow \text{OH}(v=1) + \text{OH}(v=0)$	$2.2 \times 10^{-10}$	2
$\text{O}(^1\text{D}) + \text{O}_2 \rightarrow \text{O} + \text{O}_2$	$4.0 \times 10^{-11}$	14
$\text{O}(^1\text{D}) + \text{O}_3 \rightarrow 2 \text{O}_2$	$1.2 \times 10^{-10}$	14
$\text{O}(^1\text{D}) + \text{O}_3 \rightarrow \text{O}_2 + 2 \text{O}$	$1.2 \times 10^{-10}$	14
$\text{H} + \text{O}_3 \rightarrow \text{OH}(v \leq 9) + \text{O}_2$	$2.9 \times 10^{-11}$	4-7
$\text{OH}(v=1) + \text{H}_2\text{O} \rightarrow \text{OH}(v=0) + \text{H}_2\text{O}$	$1.4 \times 10^{-11}$	15
$\text{OH}(v=1) + \text{H}_2 \rightarrow \text{OH}(v=0) + \text{H}_2$	$1.0 \times 10^{-14}$	16
$\text{OH}(v=1) + \text{O}_2 \rightarrow \text{OH}(v=0) + \text{O}_2$	$1.3 \times 10^{-13}$	17,18
$\text{OH}(v=2) + \text{Ar} \rightarrow \text{OH}(v=1) + \text{Ar}$	$<1.0 \times 10^{-14}$	19
$\text{OH}(v=2) + \text{O}_3 \rightarrow \text{HO}_2 + \text{O}_2$	$1.9 \times 10^{-12}$	20,21
$\text{OH} + \text{O}_3 \rightarrow \text{HO}_2 + \text{O}_2$	$8.2 \times 10^{-14}$	13
$\text{HO}_2 + \text{O}_3 \rightarrow \text{OH} + 2 \text{O}_2$	$2.1 \times 10^{-15}$	22
$\text{HO}_2 + \text{O} \rightarrow \text{OH} + \text{O}_2$	$5.9 \times 10^{-11}$	14
$\text{OH} + \text{O} \rightarrow \text{O}_2 + \text{H}$	$3.3 \times 10^{-11}$	14
$\text{O}_3 + \text{O} \rightarrow 2 \text{O}_2$	$8.0 \times 10^{-15}$	14
$\text{OH} + \text{OH} \rightarrow \text{H}_2\text{O} + \text{O}$	$1.9 \times 10^{-12}$	14
$\text{OH} + \text{HO}_2 \rightarrow \text{H}_2\text{O} + \text{O}_2$	$1.1 \times 10^{-10}$	14
$\text{HO}_2 + \text{HO}_2 \rightarrow \text{products}$	$1.7 \times 10^{-12}$	14
$\text{OH} + \text{H}_2 \rightarrow \text{H}_2\text{O} + \text{H}$	$6.7 \times 10^{-15}$	14

Table 3-1. Reactions occurring in the flow cell and their respective rate constants.

### 3.2 Room Temperature Results

To obtain the desired kinetic rate information, time-resolved IR absorption traces for loss of OH radical after excimer laser initiation are obtained for a wide variety of experimental conditions. To verify that the kinetic results are quantitatively reliable, these experiments have been exhaustively repeated for  $\approx 140$  different cell pressures, buffer gases, flow rates, photolysis energies, and over a 100-

fold dynamic range of ozone concentrations. An abbreviated list of the experimental conditions is summarized in table 3-2.

No. of Data Runs	Laser Energy (mJ cm <sup>-2</sup> pulse <sup>-1</sup> )	H <sub>2</sub> Pressure (Torr)	H <sub>2</sub> O pressure (Torr)	Total Pressure (Torr)	[O <sub>3</sub> ] x 10 <sup>16</sup> molecules/cm <sup>3</sup>	<i>k</i> <sub>ind</sub> (10 <sup>-14</sup> cm <sup>3</sup> /sec)
19	7.5	0	5.0	45.0	0.097 – 9.46	8.2(8)
21	4.3	0	6.6	34.9	0.25 – 7.56	8.7(8)
6	5.0	0	5.3	29.7	0.13 – 1.16	9.2(9)
21	4.9	0	4.0	24.6	0.20 – 6.45	8.3(8)
21	2.8	0	1.3	42.5	0.47 – 7.62	9.1(9)
20	1.6	0	3.3	23.4	0.42 – 6.69	8.7(8)
12	2.4	0	6.0	16.7	0.50 – 4.59	11.0(11)
19	2.6	0	12.5	43.4	0.095 – 4.52	8.0(8)
10	0.5	0	3.7	26.0	0.25 – 2.00	8.6(9)
23	0.4	0	3.8	28.0	0.50 – 3.95	8.3(8)
21	0.5	0	3.1	23.0	0.45 – 3.95	8.6(9)
18	0.5	0	3.7	27.0	0.60 – 4.05	9.3(9)
14	0.5	0	3.6	22.0	0.73 – 2.41	9.4(9)
12	0.5	1.4	0.4	26.0	0.19 – 4.00	9.2(9)
8	0.5	0	0.6	18.0	0.85 – 8.41	8.7(9)
22	0.5	12.0	3.0	25.0	0.94 – 6.52	8.7(9)
10	0.5	8.3	1.2	23.0	0.57 – 6.34	8.3(9)
8	0.5	10.0	2.8	22.0	1.02 – 5.00	8.7(9)
10	0.5	6.7	3.3	17.5	0.73 – 6.50	9.9(10)
15	0.5	0	0.5	25.0	1.00 – 6.87	10.0(10)

Table 3-2. Experimental conditions for room temperature determination of *k*<sub>ind</sub>.

A more complete discussion of these various experimental checks is deferred until later in this section. Each OH radical time trace is then fitted to the double exponential decay form predicted in equation (3.18) using nonlinear least-squares routines to extract *k*<sub>ind</sub>, *k*<sub>term</sub> and the ratio of the fast- and slow-decay components. Sample-fitted data are shown in figure 3-2, which indicate the high signal-to-noise (S/N) quality and small residuals obtained from the least-squares-fitting procedure.

From equation (3.20), these experimental conditions support over 20 complete chain cycles (i.e., more than 40 molecules of O<sub>3</sub> are destroyed for each OH radical generated photolytically). The chain induction rate component ( $k_{\text{ind}}$ ) has been plotted vs ozone concentration in figure 3-3.

From a linear least-square analysis, the slope of this fit (i.e., the induction rate constant) at 298 K is  $k_{\text{ind}} = k_1 + k_2 = 8.8(9) \times 10^{-14} \text{ cm}^3 \text{ molecule}^{-1} \text{ s}^{-1}$ , with an intercept which is negligible within uncertainty. It is worth stressing that these data reflect the results of  $\approx 200$  separate kinetic measurements, taken at over a 50-fold dynamic range in laser pulse energies and cell pressures, as well as over a 100-fold dynamic range in [O<sub>3</sub>].

Though such chain reaction kinetics have been present in previous experimental studies, the effects require relatively high S/N to see unambiguously. Furthermore, detection of the steady state chain regime is enhanced by the higher ozone concentrations accessible to the present IR method, which is able to make the initial decay rapid with respect to radical-radical chain termination processes and diffusion out of the probe beam. This is the first kinetic study of the OH/HO<sub>2</sub>/O<sub>3</sub> reaction system that takes chain propagation effects explicitly into account, and which therefore reports the sum of the two chain rate constants (i.e.,  $k_{\text{ind}} = k_1 + k_2$ ). By way of contrast, previous kinetic analyses have approximated the loss of OH as a single-exponential function of time and report a value for  $k_1$  alone.

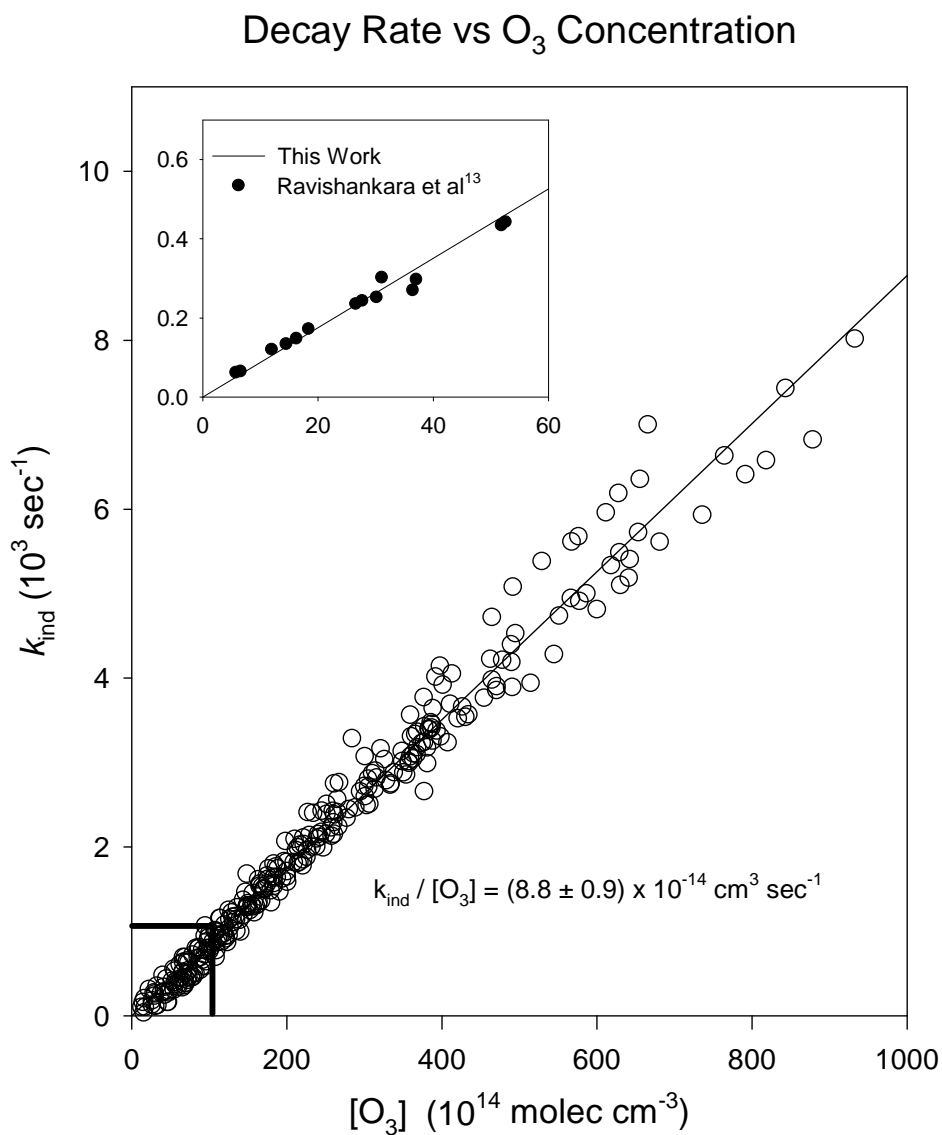


Figure 3-3. Stern-Volmer analysis of decay time vs ozone concentration at 298 K for various different experimental conditions. The slope represents the sum of the two chain rate constants,  $k_{\text{ind}} = k_1 + k_2 = 8.8(90) \times 10^{-14} \text{ cm}^3 \text{ molecule}^{-1} \text{ sec}^{-1}$ . This data reflects  $\approx 200$  different sets of independent experimental conditions taken over several months, covering (i) a 10-fold range of excimer laser intensities (0.5 – 7.5 mJ/cm<sup>2</sup>), (ii) 3-fold range of total cell pressure (16.7 – 45.0 Torr), and (iii) a 100-fold range of  $[\text{O}_3]$  ( $9.7 \times 10^{14}$  and  $9.5 \times 10^{16}$  molecules/cm<sup>3</sup>).

From the previous section, it is clear that this is not rigorously correct; for the OH/HO<sub>2</sub>/O<sub>3</sub> chain reaction system, however, the magnitude of  $k_2$  is thought to be only <5% of  $k_1$ , which explains why the second decay component would only be evident at high S/N in the previous studies. In the current studies, this double-exponential behavior is evident in all kinetic traces and is explicitly included in the kinetic analyses. Thus for consistency, the present results for  $k_{\text{ind}}$  should be compared with the earlier values reported for  $k_1$  from previous studies that presumed a purely single-exponential decay.

These results are in agreement with the previous room temperature RF studies of Ravishankara et al.,<sup>13</sup> who report a rate constant of  $8.2 \times 10^{-14} \text{ cm}^3 \text{ molecule}^{-1} \text{ s}^{-1}$ . To make this more explicit, we have replotted the Ravishankara et al. data<sup>13</sup> on top of the current data (see inset region in Figure 3-3), which indicates a nearly quantitative overlap but also under-scores the  $\approx 10$ -20 fold larger range of ozone concentrations that have been investigated via the IR laser absorption method.

Researcher	$k_{\text{ind}}[298\text{K}]$ ( $\times 10^{-14} \text{ cm}^3/\text{sec}$ )
Anderson <sup>11</sup>	$5.5 \pm 1.5$
Kurylo <sup>12</sup>	$6.5 \pm 0.5$
Ravishankara <sup>13</sup>	$8.2 \pm 0.4$
Smith <sup>23</sup>	$7.5 \pm 0.2$
Recommended Value <sup>14</sup>	6.8
This work	$8.8 \pm 0.90$

Table 3-3. Room temperature rate constants for  $k_{\text{ind}}$ .

As indicated in table 3-3, there is a relatively broad range of rate values reported in the literature<sup>11-13,23</sup>; our data is most consistent with the Ravishankara et al. value<sup>13</sup>, verified over a much larger dynamic range of [O<sub>3</sub>]. Of particular

importance, the presently determined value for  $k_{\text{ind}}$  is >20% higher than obtained from the  $k_1$  and  $k_2$  values recommended for use in atmospheric modeling.<sup>14</sup>

### 3.3 Systematic Checks

As additional confirmation of these results, the measurements have been repeated under a variety of diagnostic test conditions. The first is to assess for any effects due to nonlinear radical-radical kinetics, which one can systematically check by varying the laser power. The lack of any dependence on excimer laser power is displayed in figure 3-4, which indicate no change in the reported value of  $k_{\text{ind}}$  over a factor of 50 in laser pulse energy.

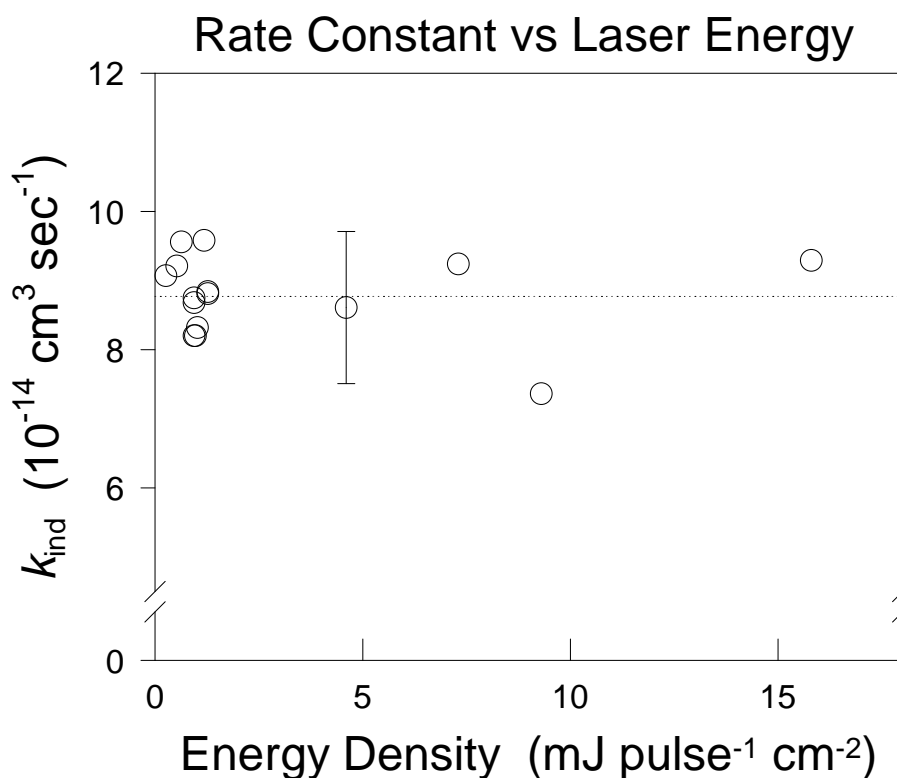


Figure 3-4. Room temperature rate constant as a function of excimer energy.

For comparison, most of the experiments reported in figure 3-3 are conducted with laser energy of  $<1 \text{ mJ/cm}^2$  at a typical ozone concentration of  $10^{16} \text{ molecules/cm}^3$ . This corresponds to an initial OH radical concentration of  $\approx 1 \times 10^{12} \text{ molecules/cm}^3$  and a  $[\text{OH}]_0/[\text{O}_3]$  ratio of  $\approx 1 \times 10^{-4}$ . This low ratio of radical to  $\text{O}_3$  concentrations ensures first-order kinetics and discriminates against contributions from even gas kinetic radical-radical reactions such as  $\text{OH} + \text{HO}_2$  on the time scale of chain reaction induction period.

A second issue to address is the degree of thermal equilibration of the OH radical. As noted by Ravishankara et al.,<sup>13</sup> this can be particularly important in the  $\text{OH}/\text{HO}_2/\text{O}_3$  chain reaction system due to acceleration of the  $\text{OH} + \text{O}_3$  chain step by OH vibrational excitation<sup>24</sup>. To eliminate these interferences, the flow cell mixture contains high concentrations of  $\text{H}_2\text{O}$ , which is an extremely efficient quencher of vibrationally as well as rotationally excited OH radical. This can be tested in several ways. First of all, this degree of internal state relaxation is confirmed in figure 3-1, which indicates the excellent temporal separation between fast OH rovibrational relaxation and the much slower removal of OH by chain reaction with  $\text{O}_3$ . Secondly, since the IR probe laser is quantum state specific, we can monitor the chain kinetics on different rotational levels, which indicate no difference within experimental uncertainty. Furthermore, these kinetic measurements have been repeated for a variety of buffer gases ( $\text{Ar}$ ,  $\text{SF}_6$ ,  $\text{N}_2$  and  $\text{O}_2$ ) and cell pressures. As displayed in figure 3-5 the observed rates are remarkably insensitive to buffer gas conditions over the full range of data represented in figure 3-3.

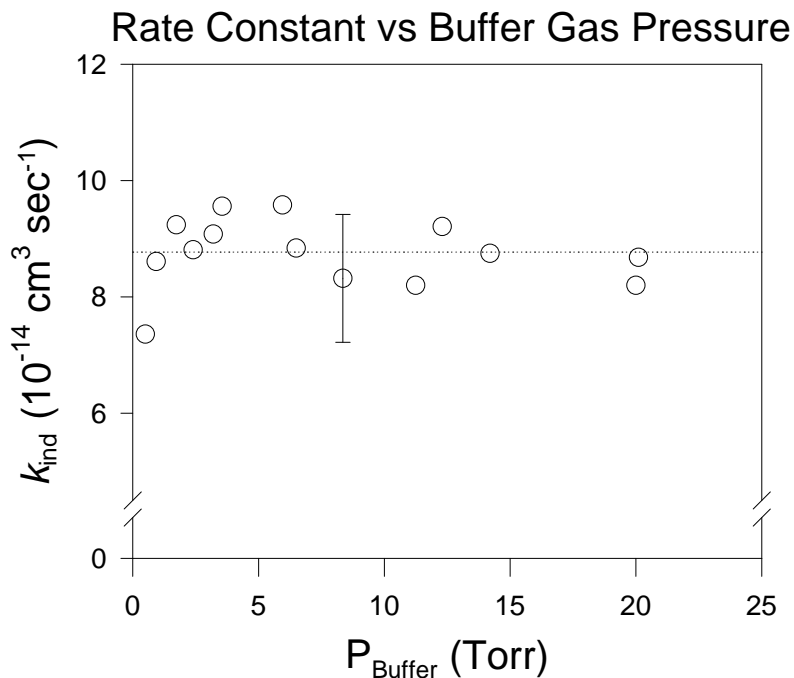


Figure 3-5. Room temperature rate constant as a function of buffer gas pressure.

### 3.4 Temperature Dependent Results

It is our goal to more fully understand the OH/HO<sub>2</sub>/O<sub>3</sub> kinetics, especially at atmospheric temperatures. The region of the atmosphere where this chain reaction is most important has an average temperature of approximately 200 K. For this reason, it is important to the scientific community to have reliable kinetic data at these temperatures. Using our flash kinetic laser apparatus, in conjunction with the temperature controlled flow cell, we are able to observe the OH/HO<sub>2</sub>/O<sub>3</sub> kinetics at various temperatures. Figure 3-7 presents the Stern-Volmer analysis for selected temperatures, while table 3-4 contains the experimental conditions and  $k_{\text{ind}}$  for these measurements.

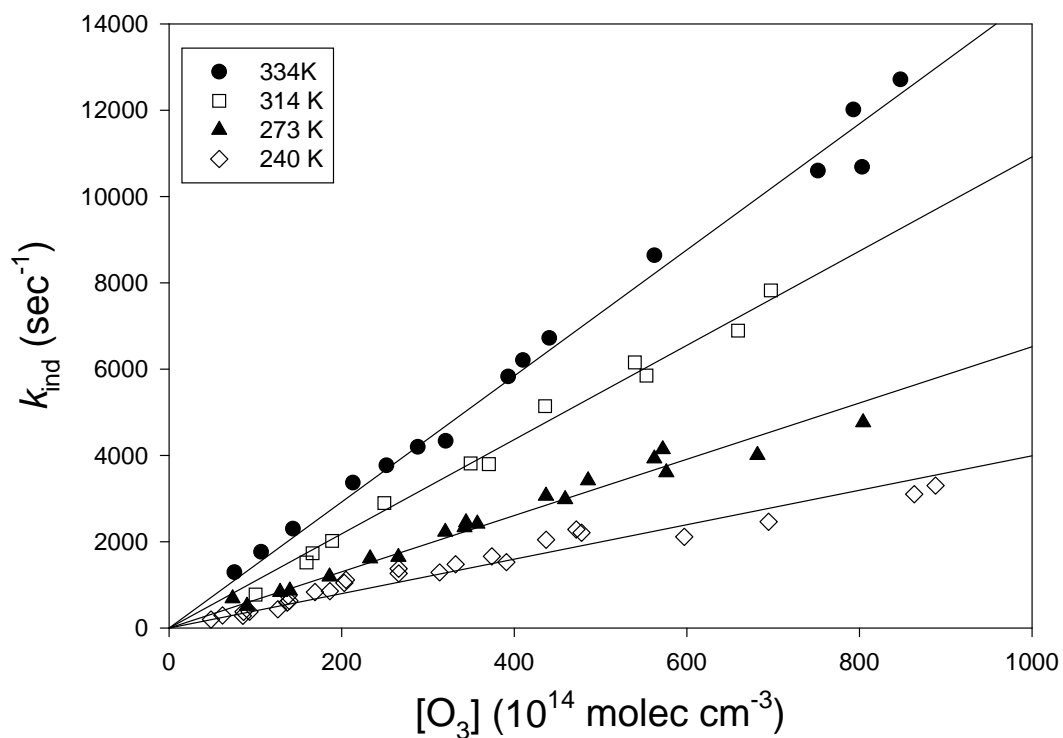


Figure 3-6. Stern-Volmer analysis of the decay time ( $k_{\text{ind}}$ ) vs ozone concentration at four temperatures: 334 K, 314 K, 273 K, and 240 K.

Temp. (K)	P[H <sub>2</sub> O] (Torr)	P[H <sub>2</sub> ] (Torr)	Total P (Torr)	$k_{\text{ind}}$ ( $\times 10^{-14}$ cm <sup>3</sup> /sec)
334(2)	4.3	0	25	14.6(14)
314(1)	4.3	0	22	10.9(11)
295(2)	0.6 – 12.0	0 – 6	16 – 42	8.94(90)
287(1)	2.5	10	22	8.28(83)
273(1)	2.5	10	22	6.52(65)
266(2)	0.3	1.0 – 1.5	20 – 25	6.20(62)
253(1)	0.3	1.0 – 1.5	25	5.16(52)
250(2)	0.3	1 – 6	25	4.60(46)
240(2)	0.3	1 – 6	23	3.99(40)

Table 3-4. Typical conditions and  $k_{\text{ind}}$  at various temperatures.

In order to determine the temperature-dependence of the rate constant for the OH/O<sub>3</sub> chain reaction, an Arrhenius expression is utilized. The Arrhenius form for a temperature dependant rate constant is as follows:

$$k(T) = A e^{-E_{\text{Act}}/T}, \quad (3.21)$$

where A is the Arrhenius pre-exponential factor, and E<sub>Act</sub> is the Arrhenius activation energy for the reaction. Using this analysis, it is common to plot the rate constant, *k*, as a function of 1/T on a semi-log graph. If the reaction conforms to the Arrhenius expression, this will yield a straight line with a slope corresponding to the Arrhenius activation energy and an intercept corresponding to the pre-exponential factor. The result of this analysis is shown in figure 3-8, with the following Arrhenius parameters:

$$k_{\text{ind}}(T) \left[ \frac{\text{cm}^3}{\text{sec}} \right] = (2.93_{-0.38}^{+0.42}) \times 10^{-12} \exp\left(\frac{-(1030 \pm 50)\text{K}}{T(\text{K})}\right). \quad (3.22)$$

Previous studies concerning the OH/O<sub>3</sub>/HO<sub>2</sub> chain reaction have been reported in the literature. For purposes of comparison, we have included these previously determined rate constants in figure 3-8. It is apparent that agreement is within experimental error at low temperatures. However, at temperatures above 300 K, our values are consistently greater than those reported. Although the Arrhenius fit is quite good in this temperature window, our Arrhenius parameters are higher than those previously determined.

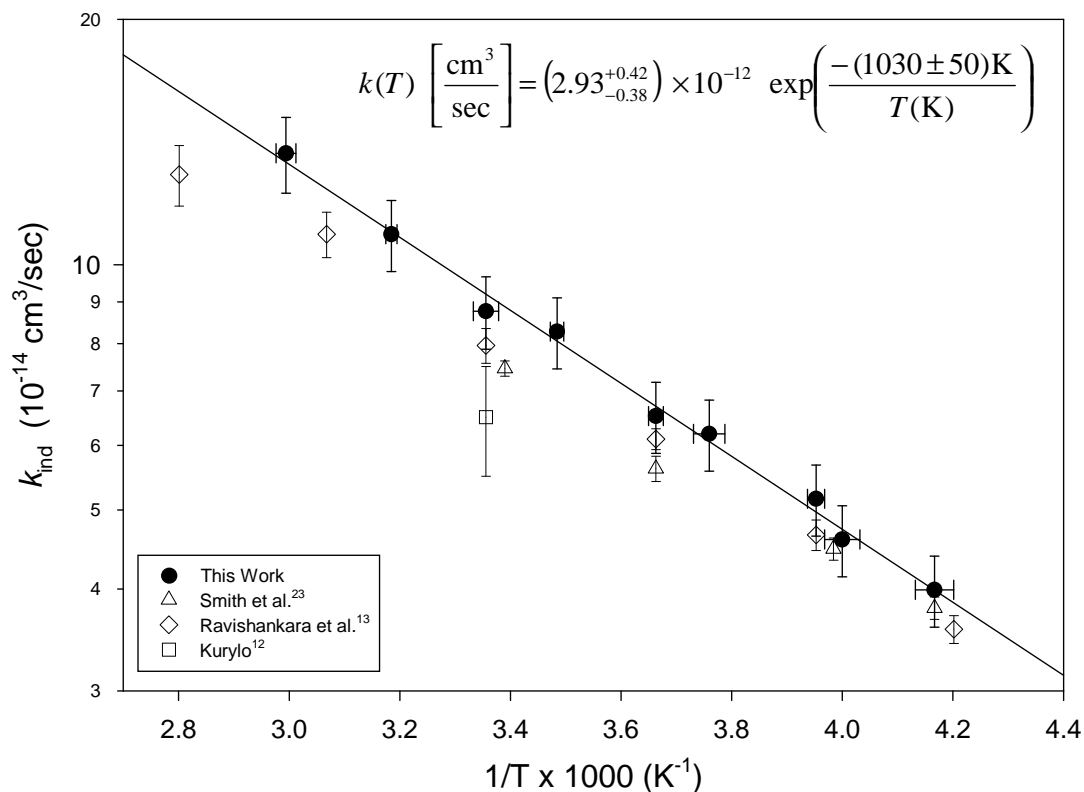


Figure 3-7. Arrhenius Plot for the induction decay rate,  $k_{\text{ind}}$ . Circles (●) represent our data, triangles (△) are from Smith et al.<sup>23</sup>, diamonds (◇) are from Ravishankara et al.<sup>13</sup>, and squares (□) are from Kurylo<sup>12</sup>.

Researcher	$k_{\text{ind}}[298\text{K}]$ ( $\times 10^{-14} \text{ cm}^3/\text{sec}$ )	A-Factor ( $\text{cm}^3/\text{sec}$ )	E/R (K)
Anderson <sup>11</sup>	$5.5 \pm 1.5$	$1.3 \times 10^{-12}$	960
Kurylo <sup>12</sup>	$6.5 \pm 0.5$	--	--
Ravishankara <sup>13</sup>	$8.2 \pm 0.4$	$(1.82 \pm 0.30) \times 10^{-12}$	$930 \pm 50$
Smith <sup>23</sup>	$7.5 \pm 0.2$	$(1.52 \pm 0.10) \times 10^{-12}$	$890 \pm 60$
Recommended Value <sup>14</sup>	6.8	$1.6 \times 10^{-12}$	$940 \pm 300$
This work	$8.8 \pm 0.90$	$(2.93 \pm 0.40) \times 10^{-12}$	$1030 \pm 50$

Table 3-5. Comparison of  $k_{\text{ind}}$  with previously determined values.

It is worth speculating what these differences might be due to. The quantity most crucial to these rate constant determinations is the ozone number density. In an effort to minimize systematic errors, we use an *in situ* measurement of ozone density by absorption of the 308 nm photolysis light. However, the accuracy of this measurement is limited to the accuracy of the known cross section and its temperature dependence. In addition, when determining the Arrhenius parameters of the reaction, the values are quite sensitive to the temperature of the reactants. Obviously, any systematic errors in temperature measurement would lead to a discrepancy. In this study, the temperature of the gas was measured directly in two places in the cell: the middle and the far end. The agreement between these measurements are within 0.5° C. In addition, we monitored the temperature of the circulating fluid, which would consistently be ~2° C colder than the gas temperature during low temperature data runs and ~1° C higher than the gas temperature during high temperature data runs. The thermocouples used in this investigation were calibrated with a mercury thermometer between 0 and 100° C and found to be accurate to 0.5%.

### **3.5 $k_2/k_{ind}$ Determination at Room Temperature**

The determination of  $k_2$  has proven to be more difficult. As presented above, the information needed to calculate  $k_2$  is contained in the long-time tail of the OH decay curve. By comparing equation (3.21) with equation (3.18), one finds that the ratio of the back extrapolated intensities is equal to  $k_2/k_{ind}$ . Hence, in order to extract both  $k_1$  and  $k_2$ , one must measure both the decay rate *and* the intensity

information. Unfortunately, intensity information is the most prone to systematic and experimental errors. In order to reduce these errors, a series of measurements were taken where special attention was paid to the determination of the ratio of  $k_2/k_{\text{ind}}$ . The result of these measurements (shown in figure 3-4) is  $k_2/k_{\text{ind}} = 0.043(2)$ . These measurements were taken at 295K only, and we are currently working to extend these measurements to lower temperatures.

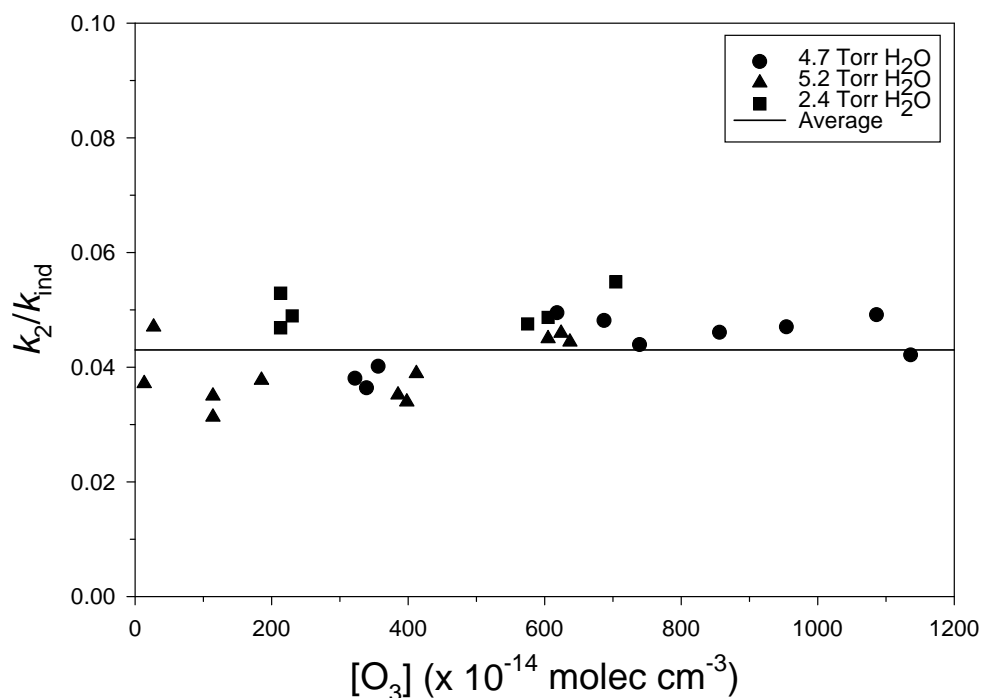


Figure 3-8.  $k_2/k_{\text{ind}}$  measurement at 295K. From this analysis, we calculate an average value to be 0.043(2).

This value can be compared with other, previous measurements of  $k_1$  and  $k_2$ . Sinha et al.<sup>22</sup> report a  $k_2/k_1$  value of 0.026(3), which is consistent with the value of 0.029(3) value of Zahniser and Howard<sup>25</sup>. As presented in the previous sections, it

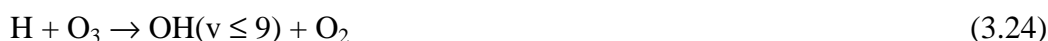
is appropriate to compare our  $k_2/k_{\text{ind}}$  to the previously measured values of  $k_2/k_1$ . Our value, however, is roughly 60% higher than these previous measurements. An explanation for this discrepancy is currently being pursued in our laboratory.

### 3.6 Breaking the 240 K Barrier

Extending the kinetic measurements below 240 K is not an easy task. At temperatures below 240 K, the vapor pressure of water becomes negligible, and the only source for OH atoms is through the reaction of O(<sup>1</sup>D) with H<sub>2</sub>.



This reaction proceeds at a gas-kinetic rate<sup>14</sup> ( $1.0 \times 10^{-10}$  cm<sup>3</sup>/sec) to form OH ( $v=0$ ). However, the product H atom can react with ozone in the cell to form vibrationally excited OH<sup>4,7</sup>.



The branching ratio of the above reaction has been studied by Charters et al.<sup>4</sup>, and more recently by Ohoyama et al.<sup>6</sup>. Ohoyama et al. has shown that 80% of the nascent vibrational distribution of OH is in  $v \geq 7$ . Without H<sub>2</sub>O present in the cell to rapidly quench the vibrationally excited OH into its ground state, its presence serves to severely complicate the kinetics. First of all, the rate of OH( $v \geq 7$ ) and O<sub>3</sub> is two orders of magnitude faster<sup>21</sup> than the rate of ground state OH. In addition, the collisional relaxation of OH( $v \geq 1$ ) by the Ar buffer gas will lengthen the initial OH rise time by two orders of magnitude. A plot of sample data where H<sub>2</sub> is the only precursor is shown in figure 3-10. One will notice the initial *emission* signal at time  $t = 0$ , signifying a population inversion with respect to the upper state, namely OH

( $v=1, J=1.5$ ). This emission signal is followed by an extremely slow rise ( $t \sim 0.5$  msec), which eventually turns around to form an exponential decay. This decay terminates to a greatly exaggerated offset, a consequence of the quickly generated  $\text{HO}_2$  product from  $\text{OH}(v \geq 9)$  and  $\text{O}_3$ .

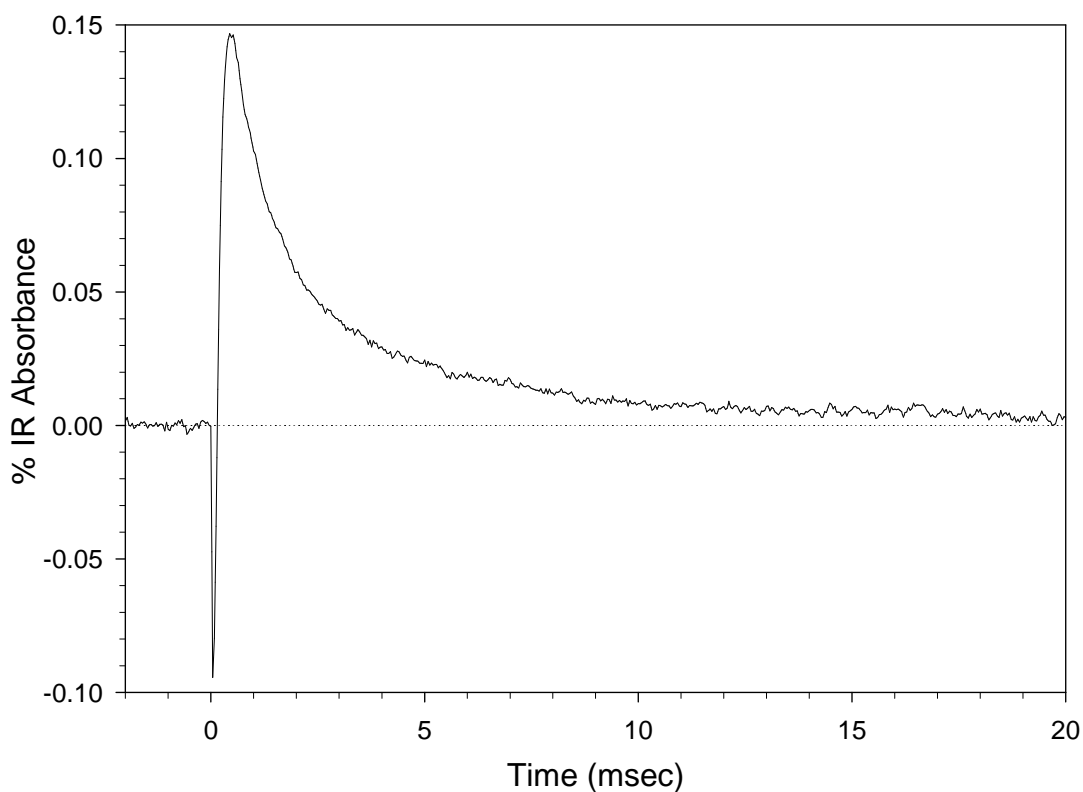


Figure 3-9. Typical OH absorption data when  $\text{H}_2$  is used as the sole precursor. This data is taken on the OH  $v=0, P(2.5)1^-$  transition. Notice the initial emission signal, indicating an initial population inversion. The slow rise time is indicative of the decreased timescale for vibrational and rotational relaxation. The conditions for this data is as follows:  $[\text{H}_2] = 12.0$  Torr,  $[\text{O}_3] = 0.30$  Torr,  $[\text{Ar}] = 17$  Torr, XeCl laser energy = 0.5 mJ/pulse.

However, it is still possible to extract the initial exponential decay and observe how the induction rate, kind, varies with respect to ozone concentration in the flow cell. The results of this analysis is shown in figure 3-11.

Temp. (K)	P[H <sub>2</sub> O] (Torr)	P[H <sub>2</sub> ] (Torr)	Total P (Torr)	$k_{\text{ind}}$ ( $\times 10^{-14}$ cm <sup>3</sup> /sec)
230(2)	0	13	30	2.38(48)
220(2)	0	12	28	2.02(40)
210(2)	0	13	30	1.44(29)
200(2)	0	12	29	0.77(15)

Table 3-6. Experimental conditions and results of OH + O<sub>3</sub> kinetic data taken below 240 K using H<sub>2</sub> as the sole precursor.

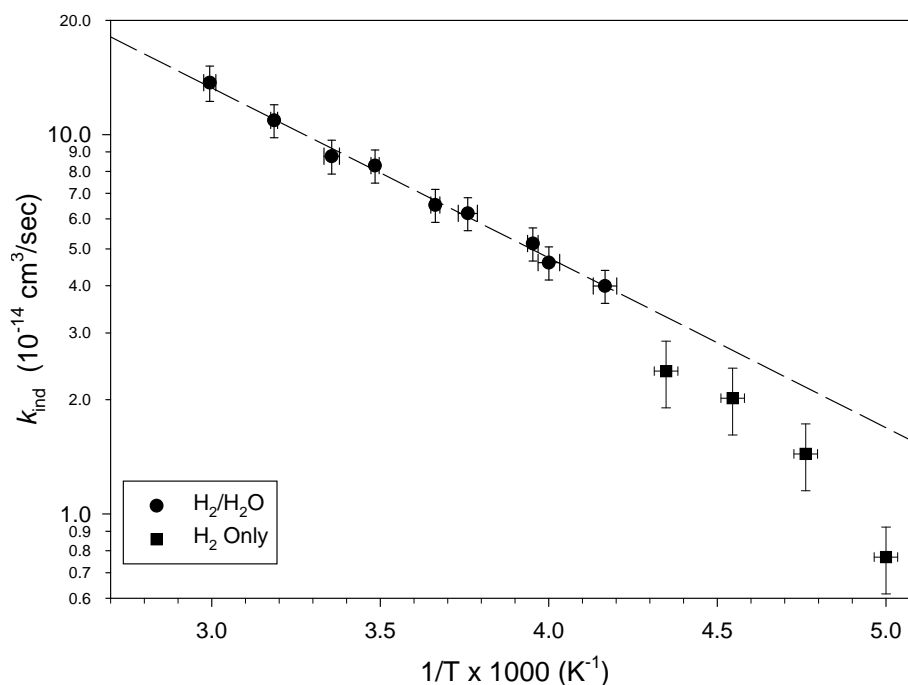


Figure 3-10. Arrhenius plot comparing data with and without H<sub>2</sub>O present in the flow cell. The decrease in rate constant when H<sub>2</sub> is used as the sole precursor is obvious in the data. A possible explanation for this discrepancy is a reaction involving H<sub>2</sub> and vibrationally excited OH.

It is obvious that a sharp break occurs in the Arrhenius plot at temperatures below 240 K. It is important to investigate possible explanations for these values

and determine how much, if at all, the rate constant,  $k_{\text{ind}}$ , is changed when  $\text{H}_2$  is the only precursor present in the cell. Ravishankara et al.<sup>13</sup> report a decrease in the reaction rate when  $\text{H}_2$  is the only precursor is present, which is consistent with the observations made in this study. Ravishankara et al. attribute the slower decay rate to a chain reaction involving vibrationally excited OH and  $\text{H}_2$ , which re-forms vibrationally excited OH:



The above reaction scheme is only active when the time scale for OH ( $v \geq 1$ ) reacting with  $\text{H}_2$  is less than the time scale for OH( $v \geq 1$ ) relaxation into OH( $v=0$ ). Spencer et al.<sup>26</sup> have studied reaction (3.25) and concluded that the rate constant for the reaction of OH( $v=1,2$ ) +  $\text{H}_2$  is  $< 1 \times 10^{-14} \text{ cm}^3/\text{sec}$ , while the rate constants for relaxation of OH( $v=1,2$ ) are  $\approx 1 \times 10^{-14} \text{ cm}^3/\text{sec}$  (see table 3.1). When we consider the high concentrations of  $\text{H}_2$  in the cell, which dictate the time scale for the OH( $v \geq 1$ ) +  $\text{H}_2$  reaction, it very possible that this chain will play a role in complicating the OH +  $\text{O}_3$  kinetics. In order for this chain to be negligible under the conditions of this experiment, the rate of reaction 3.25 must be  $< 1 \times 10^{-15} \text{ cm}^3/\text{sec}$ . Therefore, if the rate constant of reaction 3.25 is between  $1 \times 10^{-15}$  and  $1 \times 10^{-14} \text{ cm}^3/\text{sec}$ , then we would expect complications due to the chain reaction presented above.

### **3.7 Conclusion**

The primary thrust of this work has been to determine the temperature dependant rate constant of ozone depleting chain reaction involving OH and  $\text{HO}_2$ ,

by utilizing direct infrared absorption. A pseudo first order kinetic analysis is presented which correctly predicts the OH time dependence to be double exponential, with an initial exponential component determined by the sum of the two chain rate constants (i.e.  $k_{\text{ind}} = k_1 + k_2$ ). Furthermore, this chain “induction” feature decays to a nonzero OH concentration in the steady-state chain propagation regime, which is also confirmed by experimental results. This analysis differs from the previous LIF/RF studies of OH + O<sub>3</sub>, which neglect chain effects due to the HO<sub>2</sub> + O<sub>3</sub> reaction and treat the loss of OH as a single exponential decay to zero determined only by  $k_1$ . Our data analysis yields a value for  $k_{\text{ind}}$  which is confirmed over a much higher dynamic range of ozone concentrations than previously accessible by LIF and RF methods.

**References for Chapter 3**

- 1 P. H. Wine and A. R. Ravishankara, *Chem. Phys.* **69**, 365 (1982).
- 2 J. E. Butler, L. D. Talley, G. K. Smith, and M. C. Lin, *J. Chem. Phys.* **74**, 4501 (1981).
- 3 J. A. Davidson, H. I. Schiff, T. J. Brown, and C. J. Howard, *J. Chem. Phys.* **69**, 4277 (1978).
- 4 P. E. Charters, R. G. Macdonald, and J. C. Polanyi, *Appl. Opt.* **10**, 1747 (1971).
- 5 J. H. Lee, J. V. Michael, W. A. Payne, and L. J. Stief, *J. Chem. Phys.* **69**, 350 (1978).
- 6 H. Ohoyama, T. Kasai, Y. Yoshimura, H. Kimura, and K. Kuwata, *Chem. Phys. Lett.* **118**, 263 (1985).
- 7 B. J. Finlayson-Pitts and T. E. Kleindienst, *J. Chem. Phys.* **74**, 5643 (1981).
- 8 J. E. Davenport, B. Ridley, H. I. Schiff, and K. H. Welge, *J. Chem. Soc. Faraday Disc.* **53**, 230 (1972).
- 9 L. C. Lee and T. G. Slinger, *J. Chem. Phys.* **69**, 4053 (1978).
- 10 G. E. Streit, C. J. Howard, A. L. Schmeltekopf, J. A. Davidson, and H. I. Schiff, *J. Chem. Phys.* **65**, 4761 (1976).
- 11 J. G. Anderson and F. Kaufman, *Chem. Phys. Lett.* **19**, 483 (1973).
- 12 M. J. Kurylo, *Chem. Phys. Lett.* **23**, 467 (1973).
- 13 A. R. Ravishankara, P. H. Wine, and A. O. Langford, *J. Chem. Phys.* **70**, 984 (1979).
- 14 W. B. DeMore, S. P. Sander, D. M. Golden, R. F. Hampson, M. J. Kurylo, C. J. Howard, A. R. Ravishankara, C. E. Kolb, and M. J. Molina, (Jet Propulsion Laboratory, Pasadena, 1994).
- 15 G. P. Glass, H. Endo, and B. K. Chaturvedi, *J. Chem. Phys.* **77**, 5450 (1982).

- 16 G. C. Light and J. H. Matsumoto, *Chem. Phys. Lett.* **58**, 578 (1978).
- 17 J. A. Dodd, S. J. Lipson, and W. A. M. Blumberg, *J. Chem. Phys.* **95**, 5752 (1991).
- 18 K. J. Rensberger, J. B. Jeffries, and D. R. Crosley, *J. Chem. Phys.* **90**, 2174 (1989).
- 19 K. N. Rensberger, J. B. Jeffries, and D. R. Crosley, *J. Chem. Phys.* **90**, 2174 (1988).
- 20 A. E. Potter, R. N. Coltharp, and S. D. Worley, *J. Chem. Phys.* **54**, 992 (1970).
- 21 R. N. Coltharp, S. D. Worley, and A. E. Potter, *Appl. Opt.* **10**, 1786 (1971).
- 22 A. Sinha, E. R. Lovejoy, and C. J. Howard, *J. Chem. Phys.* **87**, 2122 (1987).
- 23 C. A. Smith, L. T. Molina, J. J. Lamb, and M. J. Molina, *Int. J. Chem. Kin.* **16**, 42 (1984).
- 24 G. E. Streit and H. S. Johnston, *J. Chem. Phys.* **64**, 95 (1976).
- 25 M. S. Zahniser and C. J. Howard, *J. Chem. Phys.* **73**, 1620 (1980).
- 26 J. E. Spencer, H. Endo, and G. P. Glass, *16th (International) Symposium on Combustion*, 829 (1976).